Johann Wolfgang Goethe-Universität
Institut für theoretische Physik

b baryon masses from lattice QCD: computation of propagators and correlation functions

Bachelorarbeit

eingereicht am
21. August 2013

von
NILS-ERIC GÜNTHER

Betreuender Professor: Prof. Dr. Marc Wagner
Zweitgutachter: Prof. Dr. Owe Phillipsen

Abstract

I compute correlation functions corresponding to the Λ_b and the Ω_b baryon with Wilson twisted mass lattice QCD with 2 flavors of sea quarks. To that end I will derive an expression for the correlation function that can be evaluated numerically on a computer. In contrast to a recent work [1, 2], where stochastic timeslice propagators have been used, I will use the point source method to generate the light quark propagators. I will discuss the results of my computation and will compare them to the results of [1, 2]

Zusammenfassung

Ich berechne die Korrelationsfunktionen, die den Baryonen Λ_b und Ω_b entsprechen, mithilfe der "twisted Mass lattice QCD"mit 2 flavors von See-Quarks. Dazu leite ich einen Ausdruck für die Korrelationsfunktion her, der mit einem Computer numerisch ausgewertet werden kann. Im Gegensatz zu der früheren Arbeit [1, 2], in der stochastische "timeslice-Propagatoren benutzt wurden, benutze ich die "point source"Methode zur Erzeugung der Propagatoren der leichten Quarks. Anschliessend werde ich meine Ergebnisse vorstellen und sie mit den Ergebnissen aus [1, 2] vergleichen

Contents

1 Introduction

A baryon is a bound system consisting of three valence quarks. A fascinating feature of baryons and also mesons is that their masses are far larger than the sum of the masses of their individual components. For example the up and down quarks contribute less than 5% to the mass of the proton. The remaining 95% arise from the interaction of quarks and gluons inside the proton. These interactions are described by Quantum Chromo Dynamics(QCD).
In this work lattice QCD is used to compute the masses of so called bottom- or b-baryons, consisting of a bottom quark and two lighter quarks, in this case of the flavors up, down and strange. To make computations feasible the bottom quark will be considered static. Calculations on the same subject were done before in [1, 2] using so called stochastic timeslice propagators. A more recent study [3] showed that in computations for mesons, the so called point source method was performing far better than the timeslice method regarding the statistical errors of the computation. To find out whether this is also true for static baryons, I will perform computations using the point source method and compare my results with those obtained in [1, 2]
This work was done in close collaboration with another bachelor student, who focused on different aspects of the same problem. Therefore, some aspects of it, especially the derivation of the baryon creation operators used in the following, can be found in his thesis [4] in more detail.

2 QCD and lattice QCD

2.1 Quantum Chromo Dynamics

The fields used in Quantum Chromo Dynamics (QCD) are the fermionic quark fields ψ_A^c, interacting with each other via bosonic gluons A_μ, the gauge fields of QCD. In the following, capital letters A, B, C denote the spin indices, small letters a, b, c the colour indices and μ, ν the spacetime indices. The gluon field A_μ is actually of the form $A_\mu = A_\mu^a \frac{\sigma^a}{2}$, where σ^a are the generators of the SU(3) Lie-Algebra.

QCD can be defined by the action:

$$S_{QCD}\left[\psi, \bar{\psi}, A_\mu\right] = \int d^4x \; \mathcal{L}_{QCD}\left[\psi, \bar{\psi}, A_\mu\right] \tag{2.1}$$

where

$$\mathcal{L}_{QCD}\left[\psi, \bar{\psi}, A_\mu\right] = \sum_f \mathcal{L}_f\left[\psi, \bar{\psi}, A_\mu\right] + \mathcal{L}_G\left[A_\mu\right] \tag{2.2}$$

According to the gauge principle, the action S_{QCD} is constructed to be invariant under local transformations $G(x) \in \mathrm{SU}(3)$. The Lagrangian $\mathcal{L}_{\mathrm{QCD}}$ consists of the individual Lagrangians $\mathcal{L}_f$ of every fermionic field in the system (cf. [5]):

$$\mathcal{L}_f\left[\psi, \bar{\psi}, A_\mu\right] = \bar{\psi}_f \left(i\gamma_\mu D_\mu + m_f\right) \psi_f \tag{2.3}$$

$$D_\mu = \left(\partial_\mu - igA_\mu\right) \tag{2.4}$$

As the strong interaction between quarks is described by A_μ, (2.3) and (2.4) are not only dependent on the fermionic fields but on the gauge field as well. The last term in (2.2) describes the dynamics of the gauge field itself and is given by (cf. [5]):

$$\mathcal{L}_G\left[A_\mu\right] = \frac{1}{2}\mathrm{Tr}\left(F_{\mu\nu}F_{\mu\nu}\right) \tag{2.5}$$

$$F_{\mu\nu} = \partial_\mu A_\nu - \partial_\nu A_\mu - ig\left[A_\mu, A_\nu\right] \tag{2.6}$$

2.2 Path Integral Formalism

The fundamental observables calculated in this work are so called correlation functions and are of the following structure:

$$\langle\Omega|T\{\mathcal{O}_1(x_1,t_1)...\mathcal{O}_n(x_n,t_n)\}|\Omega\rangle$$

Here T denotes the time ordering operator, which orders the field operators O_n in descending order of their time argument t_n. Correlation functions can be formulated as a path integral, which is derived in great detail in [5]:

$$\langle\Omega|T\{\mathcal{O}_1...\mathcal{O}_n\}|\Omega\rangle = \frac{1}{Z}\int D\psi D\bar{\psi}DA_\mu \mathcal{O}_1...\mathcal{O}_n e^{-S_E[\psi,\bar{\psi},A_\mu]} \tag{2.7}$$

$$Z = \int D\psi D\bar{\psi}DA_\mu e^{-S_E[\psi,\bar{\psi},A_\mu]} \tag{2.8}$$

Note that on the right-hand side of (2.7), $\mathcal{O}, \Psi, \bar{\Psi}, A_\mu$ are no longer field operators but classical fields. The integration $D\psi D\bar{\psi}DA_\mu$ denotes an integration over all possible configurations of these fields:

$$D\psi D\bar{\psi}DA_\mu := \prod_{\alpha,\beta,\mu,x} D\psi_\alpha(x)D\bar{\psi}_\beta(x)DA_\mu(x)$$

Path integrals of the following type can be solved analytically using the grassmann properties of the fermionic fields $\psi, \bar{\psi}$, as described in [5]:

$$\frac{1}{Z}\int D\psi D\bar{\psi}\ \psi_\alpha\bar{\psi}_\beta e^{-\bar{\psi}_\lambda K_{\lambda\delta}\psi_\delta} = K^{-1}_{\alpha\beta} \tag{2.9}$$

As the fermionic quark action in QCD is of the form $\bar{\psi}_\lambda K_{\lambda\delta}\bar{\psi}_\delta$, the fermionic two point correlation function is also described by the following expression:

$$\begin{aligned}\langle\Omega|\psi(x_1)\bar{\psi}(x_2)(|\Omega\rangle &= \frac{1}{Z}\int D\psi D\bar{\psi}\ \psi(x_1)\bar{\psi}(x_2)e^{-\int dx^4 dy^4 \bar{\psi}(x)K(x,y)\psi(y)} \\ &= K^{-1}(x_1,x_2) \\ &\equiv\ \Delta(x_1,x_2)\end{aligned} \tag{2.10}$$

Where

$$K(x_1,x_2) = (\gamma_\mu D_\mu + m)\,\delta(x_1-x_2) \tag{2.11}$$

This two point function is called propagator (cf. [5]) and is abbreviated by Δ.

2.3 Mass determination

Consider the following correlation function with an arbitrary field operator $\mathcal{O}$

$$\langle\Omega|\mathcal{O}^\dagger(t)\mathcal{O}(0)|\Omega\rangle$$

Where the time evolution of $\mathcal{O}$ is described by:

$$\mathcal{O}(t) = e^{-Ht}\mathcal{O}(0)e^{Ht} \tag{2.12}$$

By inserting a complete set of energy-eigenstates on both sides of $\mathcal{O}(t)$, one can bring the correlation function to the following form:

$$\begin{aligned}\langle\Omega|\mathcal{O}^\dagger(t)\mathcal{O}(0)|\Omega\rangle &= \sum_n \langle\Omega|e^{Ht}\mathcal{O}^\dagger e^{-Ht}|n\rangle\langle n|\mathcal{O}|\Omega\rangle \\ &= \sum_n \langle\Omega|\mathcal{O}^\dagger|n\rangle\langle n|\mathcal{O}|\Omega\rangle e^{-(E_n-E_\Omega)t} \\ &= \sum_n |\langle n|\mathcal{O}|\Omega\rangle|^2 e^{-(E_n-E_\Omega)t}\end{aligned} \tag{2.13}$$

Note that if $|n\rangle$ and $\mathcal{O}|\Omega\rangle$ do not have the same quantum numbers, $\langle n|\mathcal{O}|\Omega\rangle$ will vanish.
If there is a finite gap between the energy states, the exponential will strongly suppress the $n > 1$ terms in the sum for larger t and, assuming ($E_0 < E_1 < E_2$ ...), for $t \to \infty$:

$$\lim_{t\to\infty} \langle\Omega|\mathcal{O}^\dagger(t)\mathcal{O}(0)|\Omega\rangle = |\langle\Omega|\mathcal{O}|0\rangle|^2 e^{-(E_0-E_\Omega)t} = C\cdot e^{-\Delta E t} \tag{2.14}$$

ΔE is the energy difference between the vacuum and and the lightest state $|0\rangle$ with the same quantum numbers as the trial state $\mathcal{O}|\Omega\rangle$. Therefore $|0\rangle$ is a single particle state with the mass ΔE. By calculating (2.12) and analyzing its time evolution, one can thus extract the mass of a particle. In practice, one can only evaluate (2.12) for finite times. Therefore the so called effective mass is used in this work:

$$m_{\text{eff}}(t) = \ln\left(\frac{C(t)}{C(t+1)}\right) \tag{2.15}$$

where

$$m = \lim_{t\to\infty} m_{\text{eff}}(t) \tag{2.16}$$

2.4 Lattice QCD

Because (2.7) cannot be solved analytically, numerical methods are used to perform path integrals. In order to do so, one has to discretize the continuous spacetime by a lattice with a finite distance a between neighbouring sites:

1. $x_\mu \to a n_\mu, \quad n_\mu \in \mathbb{Z}$
2. $\psi(x) \to \psi(n)$
3. $\int d^4x \to a^4 \sum_n$

However, discretizing A_μ breaks the gauge invariance of the action. Therefore one uses so called links:

$$U(x,y) = exp\left(ig \int_x^y dz_\mu \; A_\mu(z)\right) \tag{2.17}$$

The following notation is common:

$$U_\mu(n) \equiv U(n, n+\hat{\mu}) \tag{2.18}$$

With links, covariant derivatives on a lattice can be defined by (cf. [5]):

$$\nabla_\mu \psi(n) = \quad \tfrac{1}{a}\left(U_\mu^\dagger(n)\psi(n+\hat{\mu}) - \psi(n)\right) \tag{2.19}$$

$$\nabla_\mu^* \psi(n) = \quad -\tfrac{1}{a}\left(U_{-\mu}^\dagger(n)\psi(n-\hat{\mu}) - \psi(n)\right) \tag{2.20}$$

In the continuum limit $a \to 0$ the lattice action should converge to the continuum action (2.2). This condition leaves some amount of freedom as several such lattice actions can be constructed, which converge to S_{QCD}.

A straight forward lattice action for fermions could be:

$$S_f\left[\psi, \bar{\psi}, U\right] = a^4 \sum_n \cdot \bar{\psi}_f(n)\left(\frac{1}{2}\gamma_\mu(\nabla_\mu + \nabla_\mu^*) + m\right)\psi_f(n) \tag{2.21}$$

However, with this action additional fermionic flavors not present in the physical action arise. This is known as the fermion doubling problem. To get rid of these additional flavors an additional term, which vanishes for $a \to 0$, is added. This leads to the so called Wilson fermionic action.

$$S_F^{(W)}\left[\psi, \bar{\psi}, U\right] = \quad a^4 \sum_n \bar{\psi}(n)(D_W + m)\psi(n) \tag{2.22}$$

$$D_W = \quad \tfrac{1}{2}\gamma_\mu(\nabla_\mu + \nabla_\mu^*) + \tfrac{ar}{2}\nabla_\mu\nabla_\mu^* \tag{2.23}$$

In this work, a variant of this action, the Wilson twisted mass action is used (cf. subsection 2.5).Further details on the doubling problem can be found in [5].

As U_μ replaces A_μ on the lattice, a discretization of the gauge action (2.5) is needed in terms of link variables. A common choice for the gauge action is (cf. [5]):

$$S_G[U] = \sum_n \frac{2}{g^2} Tr\left[1 - \frac{1}{2}\left(U_{\mu\nu}(n) + U^\dagger_{\mu\nu}(n)\right)\right] \tag{2.24}$$

where $U_{\mu,\nu}$ are so called Plaquettes:

$$U_{\mu\nu}(n) = U_\mu(n) U_\nu(n+\hat{\mu}) U^\dagger_\mu(n+\hat{\nu}) U^\dagger_\nu(n) \tag{2.25}$$

Note that because of the definition of U_μ in (2.17), in the continuum limit $a \to 0$ the action $S_G[U]$ converges to the continuum gauge action defined by (2.5).

2.5 Wilson Twisted Mass Fermions

The following fermion action is the so called Wilson twisted mass action

$$S_F[\chi, \bar{\chi}, U] = a^4 \sum_n \bar{\chi}(D_W + m + i\mu\gamma_5\tau_3)\chi \tag{2.26}$$

where $\chi = (\chi_u, \chi_d)$, μ is the so-called twisted mass and τ_3 is the 3rd pauli matrix in (u,d) flavor space. This action converges in the continuum limit $a \to 0$, and after a coordinate transformation, the so called twist rotation

$$\psi = exp\left(i\frac{\omega}{2}\gamma_5\tau_3\right)\chi, \qquad \bar{\psi} = \bar{\chi}\ exp\left(i\frac{\omega}{2}\gamma_5\tau_3\right) \tag{2.27}$$

to the fermionic continuum action S_f corresponding to (2.3).

$\chi, \bar{\chi}$ are called the twisted basis and $\bar{\psi}, \psi$ physical basis. At maximal twist,corresponding to $\omega = \frac{\pi}{2}$, a computation with the twisted mass action yields discretization errors, wich are only $\mathcal{O}(a^2)$.
The twisted mass action (2.26) is only defined for flavor doublets. In order to use the twisted mass formalism for strange quarks as well, a partially quenched setup is used as in [3]. In this setup, valence strange quarks correspond to a mass degenerate twisted mass doublet:

$$s \to \mathbf{s} = \begin{pmatrix} s_+ \\ s_- \end{pmatrix} \tag{2.28}$$

Either s_+ or s_- is chosen to represent the strange quark. Note that s_+ and s_- are only identical in the continuum limit. This method only provides strange valence quarks, strange sea quarks are neglected in this work.

3 Correlation function

3.1 baryon creation operators

The baryons investigated in this thesis are mainly Ω_b and Λ_b. The operators used here to create the corresponding trial states are derived in detail in [4]. These operators are of the following general structure:

$$\mathcal{O} = \epsilon^{abc} Q^a \left((\psi_1^b)^T \mathcal{C}\Gamma(\psi_2^c) \right) \tag{3.1}$$

Q is the static bottom quark field, ψ_1, ψ_2 are the two light quark fields and $\mathcal{C} = \gamma_0\gamma_2$ is the charge conjugation matrix. Γ is a matrix in Dirac space which ensures that $\mathcal{O}|\Omega\rangle$ has the desired quantum numbers of the baryons. As a static quark spin is not involved in any interactions, the spin structure of the bottom quark will not be considered

$$Q_A^a \equiv Q^a$$
$$\bar{Q}_A^a \equiv Q^{\dagger a}$$

For the same reason it is appropriate to label the baryons with the total angular momentum j of the two light quarks. The individual quantum numbers as well as the corresponding Γ matrices are shown in table 1:

state	Γ	$\psi_1\psi_2$	P	I_z	j
Λ_b	γ_5	$ud - du$	$+$	0	0
Ω_b	γ_j	ss	$+$	0	1
bss_γ_0	γ_0	ss	$-$	0	0

Table 1: quantum numbers of investigated states, according to [4]

The last operator in the list corresponds to a state not yet observed experimentally. It will be denoted by bss_γ_0 in this work.

3.2 the correlation function

With the structure of the operators $\mathcal{O}$ known, one can evaluate (2.12):

$$C(t) = \langle\Omega|\mathcal{O}^\dagger(t)\mathcal{O}(0)|\Omega\rangle \tag{3.2}$$

The $(...)^\dagger$ operation leads to the following operator $\mathcal{O}^\dagger(t)$:

$$\begin{aligned}
\mathcal{O}^\dagger &= \epsilon^{abc}[Q^a \left((\psi_1^b)^T \mathcal{C}\Gamma(\psi_2^c) \right)]^\dagger \\
&= \epsilon^{abc}[(\psi_2^c)^\dagger (\mathcal{C}\Gamma)^\dagger (\psi_1^b)^{\dagger T} Q^{a\dagger}] \\
&= \epsilon^{abc}[(\bar{\psi}_2^c)\gamma_0(\mathcal{C}\Gamma)^\dagger\gamma_0(\bar{\psi}_1^b)^T \bar{Q}^a] \\
&= \pm\epsilon^{abc}[(\bar{\psi}_2^c)(\mathcal{C}\Gamma)^\dagger(\bar{\psi}_1^b)^T \bar{Q}^a]
\end{aligned} \tag{3.3}$$

The sign in the last step depends on Γ. A list of signs for the individual $\mathcal{O}^\dagger$ is found in table 2:

Γ	sign
γ_0	$+$
γ_1	$+$
γ_2	$-$
γ_3	$+$
γ_5	$+$

Table 2: signs of investigated $\mathcal{O}^\dagger$

This leads to the following correlation function:

$$\begin{aligned}
&C(t)\\
&= \pm\epsilon^{abc}\epsilon^{def}\Big\langle\ (\bar{\psi_2^c})_C(\mathcal{C}\Gamma)_{CB}(\bar{\psi_1^b})^T_B\bar{Q}^aQ^d(\psi_1^e)^T_E(\mathcal{C}\Gamma)_{EF}(\psi_2^f)_F\Big\rangle\\
&= \pm\epsilon^{abc}\epsilon^{def}\Big\langle\ Q^d\bar{Q}^a(\mathcal{C}\Gamma)_{CB}(\psi_1^e)^T_E(\bar{\psi_1^b})^T_B(\mathcal{C}\Gamma)_{EF}(\psi_2^f)_F(\bar{\psi_2^c})_C\Big\rangle\\
&= \pm\epsilon^{abc}\epsilon^{def}\Big\langle(\Delta_Q^{ad})(\mathcal{C}\Gamma)_{CB}(\Delta_1^{be})_{BE}(\mathcal{C}\Gamma)_{EF}(\Delta_2^{cf})_{FC}\Big\rangle_U\\
&= \pm\epsilon^{abc}\epsilon^{def}\Big\langle(\Delta_Q^{ad})\mathrm{Tr}_{Spin}(\mathcal{C}\Gamma\Delta_1^{be}\mathcal{C}\Gamma\Delta_2^{cf})\Big\rangle_U
\end{aligned} \tag{3.4}$$

I made the following abbreviation:

$$\Big\langle ... \Big\rangle \hat{=}\ \tfrac{1}{Z}\int DQD\bar{Q}D\psi_1D\bar{\psi}_1D\psi_2D\bar{\psi}_2DUe^{-S_{\mathrm{QCD}}}$$

In the third step I used (2.10) to formally integrate over all fermion fields. Therefore at the end of (3.4), the integral is no longer performed over all fields, but only over U.

$$\Big\langle ... \Big\rangle_U \hat{=}\ \frac{1}{Z}\int DUe^{-S^{\mathrm{eff}}_{\mathrm{QCD}}}$$

$$S^{\mathrm{eff}}_{\mathrm{QCD}} = S_G - \sum_f \ln(\det(K_f))$$

where K_f is the Dirac matrix defined by (2.11).

The assumption of a static bottom quark allows the use of the so called heavy quark effective theory, leading to the following static quark propagator:

$$\Delta_Q^{ab}(x,\tilde{x}) = \delta^{(3)}(\mathbf{x}-\tilde{\mathbf{x}}) \cdot U^{ab}(x,\tilde{x}) \exp(-m_Q \cdot) \tag{3.5}$$

where m_Q denotes the bottom quark mass and U^{ab} is a Schwinger integral defined in (2.17).
Because in this work only mass differences between b-baryons and the b-meson are considered, $\exp(-m_Q t)$ will be omitted. This results in the following expression for the correlation function:

$$\begin{aligned} &C(t) \\ &= \epsilon^{abc}\epsilon^{def}\left\langle U^{ad}(\tilde{\mathbf{x}},t,\tilde{\mathbf{x}},0)\mathrm{Tr}_{Spin}(\mathcal{C}\Gamma\Delta_1^{be}(\tilde{\mathbf{x}},t,\tilde{\mathbf{x}},0)\mathcal{C}\Gamma\Delta_2^{cf}(\tilde{\mathbf{x}},t,\tilde{\mathbf{x}},0))\right\rangle \end{aligned} \tag{3.6}$$

3.3 Monte Carlo simulation

The path integral in (3.6) is now of the following form:

$$\int DU\ (...)\ \frac{e^{-S_{\mathrm{QCD}}^{\mathrm{eff}}[U]}}{Z} \tag{3.7}$$

where

$$Z = \int DU e^{-S_{\mathrm{QCD}}^{\mathrm{eff}}[U]} \tag{3.8}$$

Because the dimensionality of $\int DU$ is rather large

$$DU = \prod_{n,\mu} DU_\mu(n)$$

its computation requires specific methods. Note that (3.8) is of the same form as a partition function in thermodynamics, but with $\exp(-S_{\mathrm{QCD}}^{\mathrm{eff}}[U])$ instead of the normal Boltzmann factor. In that analogy the path integral (3.7) can be considered a weighted average over an infinite set of gauge configurations:

$$\int DU\ (...)\ \frac{e^{-S_{\mathrm{QCD}}^{\mathrm{eff}}[U]}}{Z} \to \left\langle ... \right\rangle \tag{3.9}$$

where the gauge configurations are distributed by

$$\rho[U] = \frac{e^{-S_{\mathrm{QCD}}^{\mathrm{eff}}[U]}}{Z} \tag{3.10}$$

This mathematical structure is suited for Monte-Carlo algorithms based on importance sampling. A finite number of gauge configurations are generated according to ρ and are used to average over the integrand of (3.6). This yields the exact correlation function within statistical errors that scale with $\frac{1}{\sqrt{N}}$, where N is the number of configurations used.

4 Fermionic propagators

The inversions (2.11) leading to the light quark propagators are the most time consuming part in the computation of the correlation function (3.6). In general an exact computation of the full quark propagator is hardly feasible. The methods discussed in the following section are used to circumvent this problem.

4.1 Point Sources

A point source $\xi[a, A, y]^b_B(x)$ is defined as:

$$\xi[b, B, y]^a_A(x) = \delta^{(4)}(y - x) \cdot \delta^a_b \delta^A_B \tag{4.1}$$

Solving

$$D^{ab}_{AB}(x, y)\Phi[c, C, y]^b_B(x) = \xi[c, C, y]^a_A(x) \tag{4.2}$$

with respect to Φ for every $[c, C, y]$ would yield the full propagator:

$$\Delta^{bc}_{BC}(x, y) = \Phi[c, C, y]^b_B(x) \tag{4.3}$$

However, the two propagators involved in (3.6) all have the same argument $\tilde{x} = (\tilde{\mathbf{x}}, 0)$ at one end. Thus it is sufficient in this case to solve (4.2) for every $[c, C]$ only at the point $\tilde{x}$:

$$\Delta^{bc}_{BC}(x, \tilde{x}) = \Phi[c, C, \tilde{x}]^b_B(x) \tag{4.4}$$

This is called a point-to-all propagator.

4.2 Timeslice Sources

A set of stochastic timeslice sources $\xi^{a,n}_A(x)$ indexed by n at time t_0 is defined by:

$$\xi^{a,n}_A(x_1) = \delta(t_1 - t_0)\delta^a_b \delta^A_B Z^n(\mathbf{x}_1) \tag{4.5}$$

where $Z^n(\mathbf{x})$ satisfy the relation:

$$\left\langle Z^n(\mathbf{x}) Z^{m\,\dagger}(\mathbf{y}) \right\rangle = \delta^{(3)}(\mathbf{x} - \mathbf{y})\delta^m_n \tag{4.6}$$

Here $\langle ... \rangle$ denotes the average over an infinite number of samples. Used in combination with :

$$\begin{aligned} D^{ab}_{AB}(x_0, t_0, x_1, t_1)\Phi^{b,n}_B(x_1, t_1) &= \xi^a_A(x_0, t_0) & (4.7) \\ \Phi^{b,n}_B(x_1, t_1) &= (D^{ba}_{BA})^{-1}(x_1, t_1, x_0, t_0)\xi^a_A(x_0, t_0) & (4.8) \end{aligned}$$

this averaging property can be used to evaluate the propagator stochastically:

$$\begin{aligned}\left\langle \Phi_A^{a,n}(x_1,t_1)\xi_B^{b,m\,\dagger}(x_2,t_0)\right\rangle &= (D_{AC}^{ac})^{-1}(x_1,t_1,x_3,t_0) \qquad (4.9)\\ &\quad \left\langle \xi_C^{c,n}(x_3,t_0)\xi_B^{b,m\,\dagger}(x_2,t_0)\right\rangle \\ &= (D_{AB}^{ab})^{-1}(x_1,t_1,x_2,t_0) \qquad (4.10)\end{aligned}$$

As you can see in (4.10), the propagator calculated is the propagator from any spatial argument $\mathbf{x}_2$ to any spacetime point $(\mathbf{x}_1, t_1)$. That is why (4.10) is called timeslice propagator.

4.3 Comparison

As the correlation function (3.6) is independent of $\tilde{\mathbf{x}}$, the correlation function can be averaged over all spatial points $\tilde{\mathbf{x}}$ using timeslice propagators:

$$\tilde{C}(t) = \sum_{\tilde{\mathbf{x}}} C[\tilde{\mathbf{x}}](t) \qquad (4.11)$$

With (4.11), all the statistical information stored in a single configuration is used, whereas the point source method evaluates the gauge configuration only at a single spatial point. Therefore the gauge noise in (3.6), the error due to the fluctuations of the gauge configurations, can be greatly reduced with timeslice propagators compared to point propagators.
On the other hand, the average in (4.10) can only be performed on a finite number of samples in practice. Therefore timeslice propagators contain a stochastic noise while the point source method yields exact propagators.
So all in all, by using the timeslice method one accepts additional noise in the propagators compared to the point source method to reduce the gauge noise in the correlation function. It is investigated in section 6 whether this trade-off is beneficial or not.

5 Simulation Details

All computations leading to the results in section 6 were performed on the "CSC Fuchs" cluster in Frankfurt.

5.1 Lattice Setup

The 24 gauge configurations used in this work were generated by the ETM Collaboration on a lattice with the dimensions $T = 48$, $L_x = L_y = L_z = 24$ and $N_f = 2$ flavors of sea quarks. For fermions the wilson twisted mass action was used with twisted masses $\mu_{u/d} = 0.004$ for up and down quarks, corresponding to a pion mass of $m_\pi = 336MeV$ and $\mu_s = 0.022$ for strange quarks, corresponding roughly to physical mass. The maximal twist was $\kappa = 0.160856$. The gauge action used is the tree-level Symanzik-action described in [6]. the lattice spacing was $a = 0.079$fm, which corresponds to $\beta = 3.9$ used in the generation of gauge configurations.

5.2 Smearing

Smearing is an expression for techniques which improve the numerical behavior of the trial state. In this work, the static propagators were smeared with the HYP2-technique to decrease the self energy of the static quark. To get a better overlap of the trial state with the low lying energy eigenstates, spatial links were APE-smeared with the parameters $N_{\mathrm{APE}} = 40$, $\alpha_{\mathrm{APE}} = 0.5$ and Gaussian smearing was used on the light quark fields with $N_G = 90$ and $\kappa_G = 0.5$. Further details on smearing can be found in [7].

6 Numerical results

As mentioned before, this work was done in close collaboration with another bachelor student, who focused on different aspects of the same problem. Therefore some of the results presented here can also be found in his thesis [4]. The states investigated were those listed in table 1, the correlation functions of the corresponding operators are plotted in figure 1:

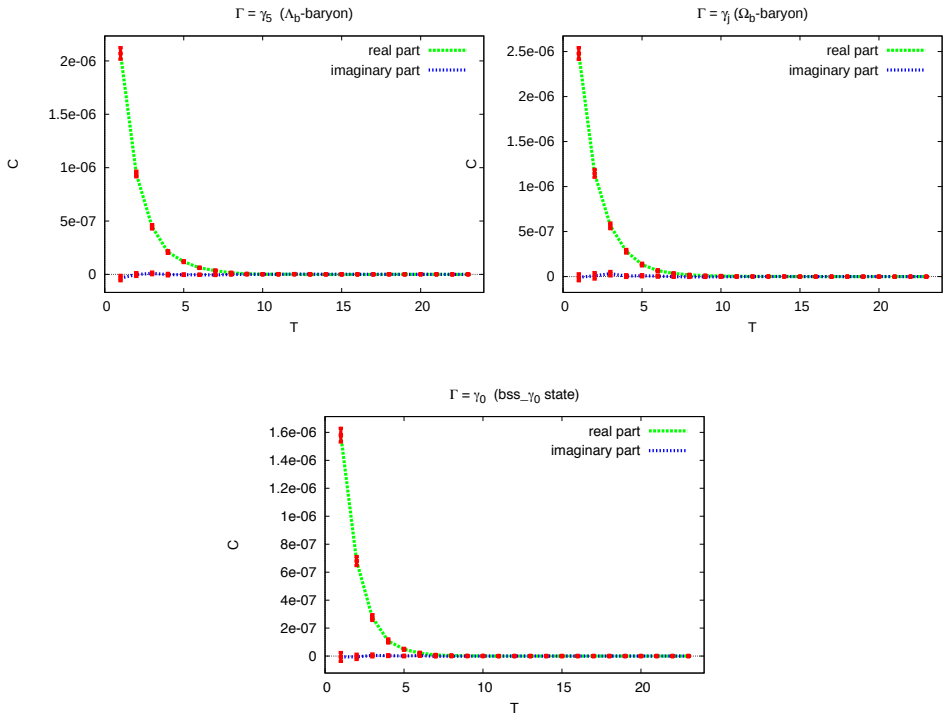

Figure 1: real and imaginary part of the two point correlation function for Λ_b, Ω_b and bss_γ_0

Note that in all cases, the imaginary part of the correlation function vanishes within statistical fluctuations. This is expected, as it is shown analytically in [1] that the correlation functions computed in this work are real valued. Thus, in the further analysis the imaginary part of the correlation functions will not be considered.

The plots in figure 2 show the masses extracted with (2.15). Fits on the effective masses of Λ_b and Ω_b once for $(2 < t < 4)$ and once for $(4 < t < 7)$ are depicted as well.

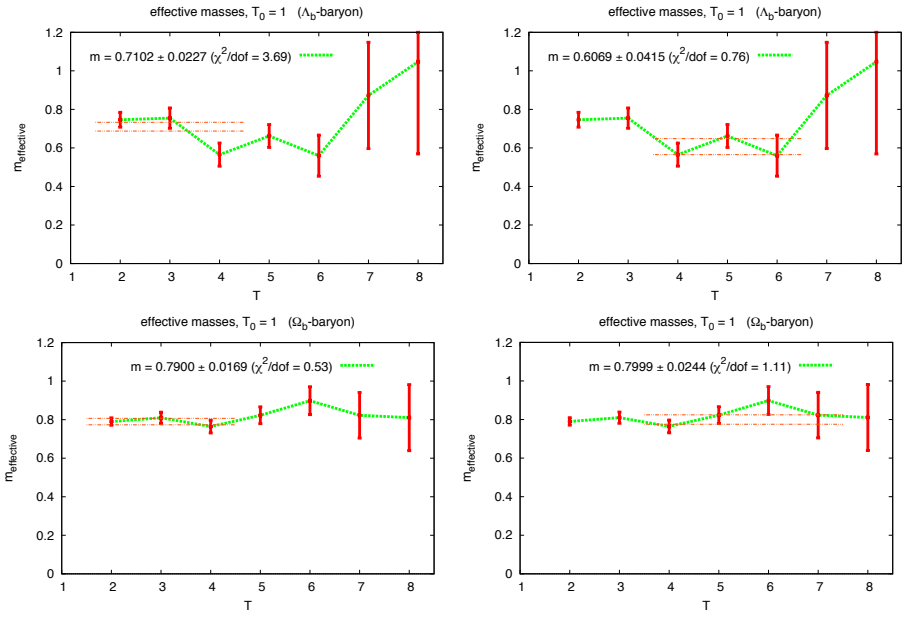

Figure 2: effective mass plot for Λ_b and Ω_b with mass fit for smaller (left) and greater (right) time regimes

Fluctuations of m_{eff} are large on both states and a precise identification of a plateau seems not possible. Especially the extracted mass of Λ_b is changing considerably during time evolution. Possibly the suppression of exited states required in (2.14) is not as strong for Λ_b as for Ω_b, as it involves lighter quarks.

The main goal of this work was to investigate whether the point source method is performing better than the timeslice method used in [1, 2] regarding their statistical errors. Thus in the following, a detailed comparison of the results of both works is presented. The results in [1, 2] were computed with the same parameters used in this work. Therefore both computations should yield the same results within errors. A direct comparison of the correlation functions computed in this work and in [1, 2] can be found in figure 3:

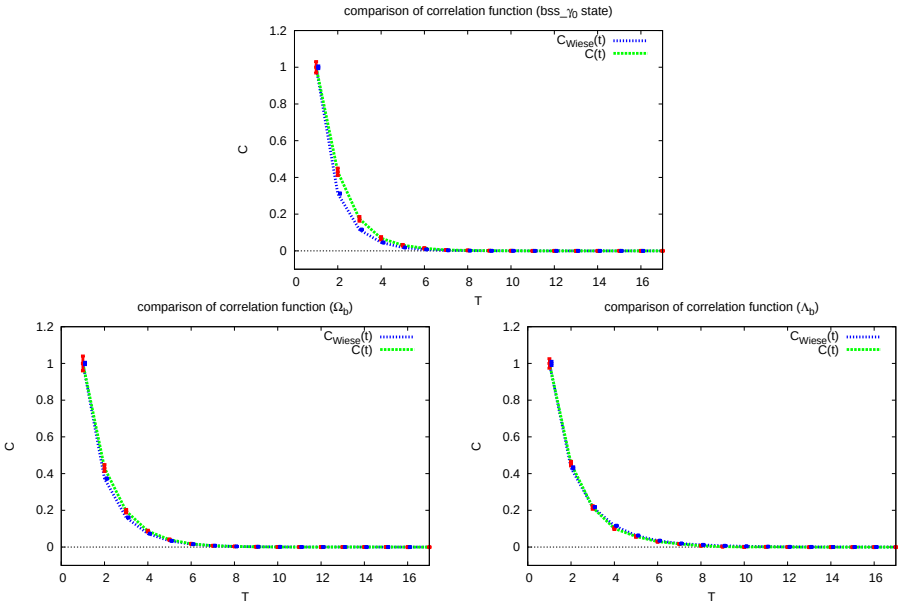

Figure 3: comparison of the correlation functions derived in this work and in [1, 2]

A comparison of the extracted masses can be seen in table 3.

state	$a \cdot m$ in [1, 2]	$a \cdot m$	$m - m_B$ in [1, 2]	$m - m_B$
Λ_b	0.5863 ± 0.0085	0.6069 ± 0.0415	461(24)MeV	512(103)MeV
Ω_b	0.7482 ± 0.0034	0.7999 ± 0.0244	865(8)MeV	994(60)MeV

Table 3: comparison of the effective masses m obtained in this work and those in [1, 2]

Despite the small number of gauge configurations used, it seems as both correlation functions and extracted masses are roughly consistent within errors. Computations in [1, 2] werde performed with the same amount of inversions per configuration as in this work. However, the number of samples used in [1, 2] to calculate the correlation functions were far larger than in this work for every computed state:

- Λ_b: $N_1 = 23$ configurations were used in this work, while $N_2 = 200$ samples were used in [1, 2].
- Ω_b: $N_1 = 24$ configurations were used in this work where 200 were used in [1, 2]. Additionally, computations in [1, 2] averaged over s_+ and s_- in (2.28), effectively yielding $N_2 = 400$ samples.

- *bss* γ_0: $N_1 = 24$ configurations were used in this work while 200 samples were used in [1, 2]. Computations in [1, 2] averaged over s_+ and s_- in (2.28), amounting to effectively $N_2 = 400$ samples. Moreover computations on *bss* γ_0 in this work were done only in positive time directions in contrast to all other computations both in this work and in [1, 2]. This yields an additional factor of 2 in the error ratio.

According to the central limit theorem, the error in Monte-Carlo simulations is $\propto \frac{1}{\sqrt{N}}$, where N is the number of samples. Therefore, if both methods would have equal performance regarding their relative errors ΔC_1 and ΔC_2, the following would apply:

$$\frac{\Delta C_1}{\Delta C_2} = \sqrt{\frac{N_2}{N_1}} \tag{6.1}$$

The numerically found ratios are shown in figure 4

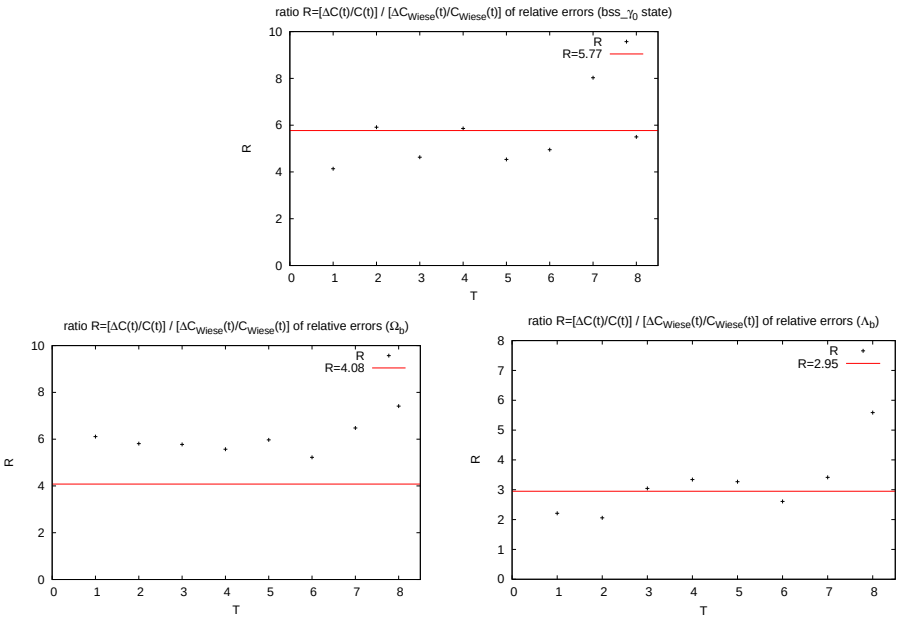

Figure 4: ratio of relative errors of correlation functions derived in this work and in [1]

As the relative errors of both computations and therefore also fluctuations within the errors, wich have not been computed yet, increase for larger t, ratios for small t in table 4 can be considered the most reliable. The favorable method seems to depend on the investigated state:

- Λ_b: the point source results here seem to be slightly better than the timeslice results. At small time separations, the ratio is under the estimated benchmark (6.1) for equal performance.

- Ω_b: the ratios indicate that the point propagators performed slightly worse compared to timeslice propagators.
- $bss\ \gamma_0$: The fluctuation of ratios is rather high even for small times, making a reliable statement difficult. However the ratios are always below or close to the benchmark (6.1), indicating a slightly better performance of the point source method.

The results are somewhat surprising, as the point propagator performance is the worst for Ω_b and the best for Λ_b while the point propagators were expected to be the most efficient method heavier quarks, just like in [2]. This outcome might be due to the different spin structure of Ω_b and Λ_B, but reliable conclusions cannot be made without further investigation, especially of the error of the ratios in figure 4. In the case of bss_γ_0, the ratio of errors is not precise enough to make a strong statement. A computation with a higher number of samples would reduce the error and therefore the fluctuation within the error as well, maybe making a more robust statement possible.

7 Discussion

This first comparison of the two inversion methods shows that none of the two methods seem to be strongly superior. It is a remarkable outcome that the state where the point source method yielded smaller errors was Λ_b and not Ω_b. To make more reliable statements about the performance of the different methods, calculations with a far higher number of gauge configurations must be made, as the number of samples used in this work was rather small, yielding poor statistics. This would also allow a serious comparison of calculated masses with physically measured masses as can be found in the Particle Data Book [8]. Furthermore, it would be reasonable to calculate correlation functions for far more trial states than used here, so an evaluation is not restricted to only three cases and one is able to gain a more comprehensive picture of the quantum numbers and states where one method is favorable to the other.

References

[1] Christian Wiese. The Spectrum of Static-light Baryons in Twisted Mass Lattice QCD. bachelor thesis, Humboldt-Universität zu Berlin, July 2010.

[2] C. Wiese M. Wagner. The static-light baryon spectrum from twisted mass lattice QCD. *Journal of High Energy Physics*, april 2011.

[3] Christian Wiese. Efficient computation of meson and four-quark correlation functions. Master thesis, Humboldt-Universität zu Berlin, September 2012.

[4] Donald Youmans. b baryon masses from lattice QCD: creation operator and quantum numbers. bachelor thesis, Johann Wolfgang Goethe-Universität Frankfurt am Main, 2013.

[5] Heinz J. Rothe. *Lattice Gauge Theories: An Introduction*, volume 82. World Scientific Publishing Co. Pte. Ltd., 4th edition, 2012.

[6] Andrea Shindler. Twisted mass lattice QCD. *Physics Reports*, 461(Issue 2-3):37–110, May 2008.

[7] M.Wagner K.Jansen. The static-light meson spectrum from twisted mass lattice qcd. *http://arxiv.org/pdf/0810.1843v1.pdf*, 2008.

[8] Particle Data Group. Particle Phyisics Booklet. Booklet, July 2012.

Selbstständigkeitserklärung

Hiermit erkläre ich, dass ich die vorliegende Arbeit selbstständig verfasst und keine anderen als die angegebenen Quellen verwendet habe.

Frankfurt am Main, den 21. August 2013

Nils-Eric Günther